

Rapid Single-Shot Measurement of a Singlet-Triplet Qubit

C. Barthel,¹ D. J. Reilly,^{1,2} C. M. Marcus,¹ M. P. Hanson,³ and A. C. Gossard³

¹*Department of Physics, Harvard University, 17 Oxford Street, Cambridge, Massachusetts 02138, USA*

²*School of Physics, University of Sydney, Sydney, 2006, Australia*

³*Materials Department, University of California, Santa Barbara, California 93106, USA*

(Received 2 February 2009; published 14 October 2009)

We report repeated single-shot measurements of the two-electron spin state in a GaAs double quantum dot. The readout allows measurement with a fidelity above 90% with a $\sim 7 \mu\text{s}$ cycle time. Hyperfine-induced precession between singlet and triplet states of the two-electron system are directly observed, as nuclear Overhauser fields are quasistatic on the time scale of the measurement cycle. Repeated measurements on millisecond to second time scales reveal the evolution of the nuclear environment.

DOI: 10.1103/PhysRevLett.103.160503

PACS numbers: 03.67.Lx, 73.63.Kv

Qubits constructed from spin states of confined electrons are of interest for quantum information processing [1], for investigating decoherence and controlled entanglement, and as probes of mesoscopic nuclear spin environments. For logical qubits formed from pairs of electron spins in quantum dots [2], several requirements for quantum computing [3] have been realized [4–7]. To date, however, measurements of these systems have constituted ensemble averages over time, while protocols for quantum control, including quantum error correction, typically require high-fidelity single-shot readout. Coherent evolution conditional on individual measurement outcomes can give rise to interesting nonclassical states [8,9]. Rapidly repeated single-shot measurements can also give access to the dynamics of the environment, allowing, for instance, feedback-controlled manipulation of the nuclear state. Single-shot measurements of solid-state quantum systems have been reported for superconducting qubits [10], the charge state of a single quantum dot [11], the spin of a single electron in a quantum dot in large magnetic fields [12,13], and the two-electron spin state in a single quantum dot [14].

In this Letter, we demonstrate rapidly repeated high-fidelity single-shot measurements of a two-electron spin (singlet-triplet) qubit in a double quantum dot. Singlet and triplet spin states are mapped to charge states [4], which are measured by a radio-frequency quantum point contact (rf-QPC) that is energized only during readout. The measurement integration time required for $>90\%$ readout fidelity is a few microseconds. On that time scale, nuclear Overhauser fields are quasistatic, leading to observed periodic precession of the qubit. By measuring over longer times, the evolution of the Overhauser fields from milliseconds to several seconds can be seen as well. We apply a model of single-shot readout statistics that accounts for T_1 relaxation, and find good agreement with experiment. Finally, we examine the evolution of the two-electron spin state at the resonance between the singlet (S) and the $m = +1$ triplet (T_+) via repeated single-shot measurement, and show that the transverse component of the

Overhauser field difference is *not* quasistatic on the time scale of data acquisition, as expected theoretically.

The double quantum dot is formed by Ti/Au depletion gates on a GaAs/ $\text{Al}_{0.3}\text{Ga}_{0.7}\text{As}$ heterostructure with a two-

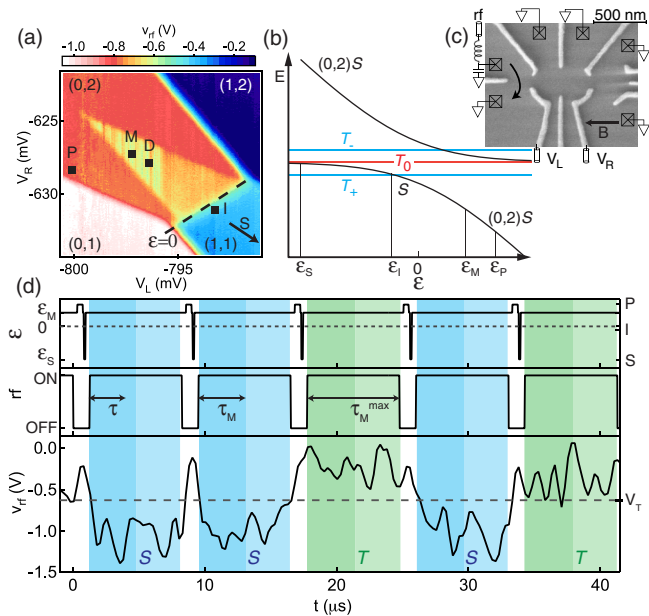


FIG. 1 (color online). (a) Charge occupancy (left, right) of the double dot, detected using rf-QPC reflectometer voltage v_{rf} in continuous-sensing mode [7] rather than single-shot readout. The triangle in (0,2) indicates where charge state (1,1) is metastable. Markers indicate gate voltages used in single-shot mode. Preparation of (0,2) singlet (P); separation for $S - T_0$ mixing (S) and $S - T_+$ mixing (I); measurement (M); operating point with 0 V pulse amplitude (D). (b) Two-electron energy levels as a function of detuning ϵ from (0,2)–(1,1) degeneracy. (c) Micrograph of device identical to measured device, indicating Ohmic contacts (boxes), fast gate lines, reflectometry circuit, grounded contacts, and field direction. (d) Pulse sequence of ϵ , controlled by V_R and V_L , cycling through the points P , S , M . Sensor signal v_{rf} indicates triplet (green, marked T) or singlet (blue, marked S) outcome for $\tau_S = 100$ ns. Integration subinterval time τ_M chosen in postprocessing.

dimensional electron gas (density $2 \times 10^{15} \text{ m}^{-2}$, mobility $20 \text{ m}^2/\text{Vs}$) 100 nm below the surface. In order to split the three triplets, an in-plane magnetic field, B , larger than the typical Overhauser fields is applied along the line between dot centers. Except where noted, $B = 200 \text{ mT}$. As described elsewhere [15], a proximal radio-frequency quantum point contact is sensitive to the charge state of the double dot, yielding an output signal v_{rf} via reflectometry, with submicrosecond time resolution. The charge state of the double dot is controlled by fast-pulsed gate voltages V_L and V_R from two synchronized Tektronix AWG710B arbitrary waveform generators.

Energy levels of the system as a function of detuning, ϵ , from the (1,1)–(0,2) charge degeneracy (controlled by V_R and V_L) are shown in Fig. 1(b). The qubit comprises the two-electron singlet (S) and $m = 0$ triplet (T_0) of the (1,1) charge state [4]. A pulse cycle [Fig. 1(d)] first prepares a spin singlet in (0,2) by waiting at point P [near the edge of (0,2)] for $\tau_P = 400 \text{ ns}$, then moving to a separation point S (I), where S and T_0 (S and T_+) are nearly degenerate, for a time τ_S (τ_I). Finally the system is brought to the measurement point M for a time τ_M^{max} . If the separated electrons are in a singlet configuration when the system is pulsed to M , the system will return to (0,2), which will be detected by the rf-QPC. If the two electrons are in a triplet state, they will remain in (1,1) at point M , and detected accordingly. Coherent superpositions will be projected to the corresponding charge state during measurement. The rf-QPC is only energized during readout, at point M [Fig. 1(d)].

The rf-QPC conductance is $\sim 5\%$ higher in (0,2) than in (1,1), yielding a charge sensitivity of $6 \times 10^{-4} e/\text{Hz}^{-1/2}$, i.e., unity signal-to-noise after 400 ns of integration. To increase fidelity, single-shot outcomes are averaged over a subinterval τ_M of the full measurement time τ_M^{max} , $V_{\text{rf}} = 1/\tau_M \int_0^{\tau_M} v_{\text{rf}}(\tau) d\tau$. By designating a threshold voltage V_T , outcomes can be classified as singlet for $V_{\text{rf}} < V_T$ or triplet otherwise. Optimization of τ_M and V_T is described below.

Figure 2(a) shows 7000 consecutive one-shot measurements of the $S - T_0$ qubit with τ_S ranging from 1–200 ns, stepped by $\sim 6 \text{ ns}$ every 200 cycles. For these data, the integration subinterval, $\tau_M = 7 \mu\text{s}$, was roughly half of the full measurement time, $\tau_M^{\text{max}} = 15 \mu\text{s}$. The histogram of single-shot outcomes [Fig. 2(b)], with voltage bin width $V_{\text{bin}} \sim 10 \text{ mV}$, is bimodal, with one peak at V_{rf}^S , corresponding to the singlet [(0,2) charge state] outcome, and the other peak at V_{rf}^T , corresponding to the triplet [(1,1) charge-state] outcome. The splitting $\Delta V_{\text{rf}} = V_{\text{rf}}^T - V_{\text{rf}}^S$ reflects the difference in output of the rf-QPC between (0,2) and (1,1) charge states, while the width σ of the two peaks reflects measurement noise [15]. However, the histogram is not simply the sum of two noise-broadened Gaussians, because some states in (1,1) decay (with relaxation time T_1 [16]) during the measurement subinterval. We model the full histogram $N(V_{\text{rf}}) = N_{\text{tot}}[n_S(V_{\text{rf}}) + n_T(V_{\text{rf}})]V_{\text{bin}}$ as the sum of probability densities of singlet outcomes,

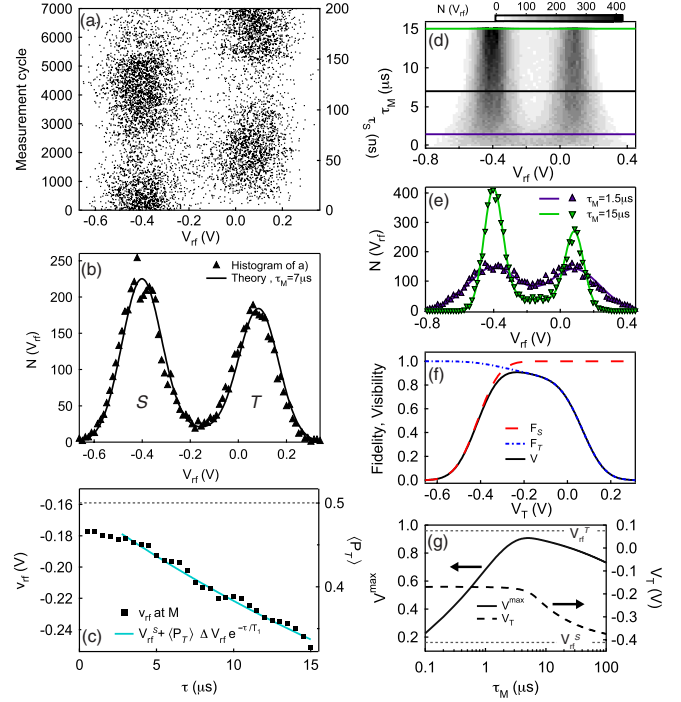


FIG. 2 (color online). (a) 7000 consecutive single-shot measurements of V_{rf} using the pulse sequence in Fig. 1(d) with integration subinterval $\tau_M = 7 \mu\text{s}$ and separation time, τ_S , incremented every 200 cycles [26]. (b) Histogram of the outcomes in (a), along with model (solid curve) [18]. (c) Instantaneous rf-QPC output $v_{\text{rf}}(\tau)$ at time τ following pulsing to M , averaged over all cycles, along with a fit to the model, giving $T_1 = 34 \mu\text{s}$ [18]. (d) Histograms $N(V_{\text{rf}})$ (gray scale) for varying τ_M . (e) Horizontal cuts through (d) along with model, with values of the parameters V_{rf}^S , V_{rf}^T from a fit to the $\tau_M = 15 \mu\text{s}$ data [18]. (f) Fidelity of singlet, F_S , and triplet, F_T , and visibility $V = F_S + F_T - 1$ as a function of threshold, V_T , for data in (b). (g) Maximum visibility, V^{max} , and optimal threshold, V_T , as a function of measurement time, τ_M .

$n_S(V_{\text{rf}})$, and triplet outcomes, $n_T(V_{\text{rf}})$, with N_{tot} the total number of measurements. The singlet probability density is modeled as a noise-broadened Gaussian around V_{rf}^S ,

$$n_S(V_{\text{rf}}) = (1 - \langle P_T \rangle) e^{-[(V_{\text{rf}} - V_{\text{rf}}^S)^2 / 2\sigma^2]} \frac{1}{\sqrt{2\pi}\sigma}, \quad (1)$$

where $\langle P_T \rangle$ is the triplet probability over all N_{tot} outcomes. Triplet outcomes, on the other hand, can take on values spread between V_{rf}^S and V_{rf}^T (and beyond, including measurement noise) to account for relaxation during the subinterval τ_M ,

$$n_T(V_{\text{rf}}) = e^{-\tau_M/T_1} \langle P_T \rangle e^{-[(V_{\text{rf}} - V_{\text{rf}}^T)^2 / 2\sigma^2]} \frac{1}{\sqrt{2\pi}\sigma} + \int_{V_{\text{rf}}^S}^{V_{\text{rf}}^T} \frac{\tau_M}{T_1} \langle P_T \rangle e^{-[(V - V_{\text{rf}}^S) / \Delta V_{\text{rf}}](\tau_M/T_1)} \times e^{-[(V_{\text{rf}} - V)^2 / 2\sigma^2]} \frac{dV}{\sqrt{2\pi}\sigma}. \quad (2)$$

The T_1 relaxation of the (1,1) triplet can be measured directly from the instantaneous rf-QPC output, $v_{\text{rf}}(\tau)$, as a function of time τ following pulsing to point M [Fig. 2(c)]. A fit of the ensemble-averaged rf-QPC output to the exponential form $v_{\text{rf}}(\tau) = V_{\text{rf}}^S + \langle P_T \rangle \Delta V_{\text{rf}} e^{-\tau/T_1}$ yields $\langle P_T \rangle = 0.5$ and $T_1 = 34 \mu\text{s}$, using values for V_{rf}^S and ΔV_{rf} determined from a fit of the $N(V_{\text{rf}})$ model to the $\tau_M = 15 \mu\text{s}$ histogram data [17].

The tradeoff for optimizing the integration subinterval τ_M is evident in Fig. 2(d), which shows histograms for a range of τ_M from 0.25 to 15 μs . For short τ_M , the two peaks are blurred due to measurement noise; for long τ_M , the triplet peak loses strength due to relaxation. To optimize readout, we first define fidelities F_S and F_T of the pure singlet ($P_T = 0$) and pure triplet ($P_T = 1$),

$$F_S = 1 - \int_{V_T}^{\infty} n_S(V) dV, \quad F_T = 1 - \int_{-\infty}^{V_T} n_T(V) dV, \quad (3)$$

following Ref. [12]. The integrals in Eq. (3) are the probabilities of misidentifying a singlet as a triplet and vice versa. Figure 2(f) shows these fidelities as well as the visibility, $V = F_S + F_T - 1$, for the $\tau_M = 7 \mu\text{s}$ data [from Fig. 2(b)] as a function of the threshold voltage V_T . For this value of τ_M , the maximum visibility, $\sim 90\%$, is achieved for V_T slightly less than the mean of V_{rf}^T and V_{rf}^S so that a triplet decaying towards the end of τ_M still gets counted correctly. Optimal thresholds V_T , along with their associated maximum visibilities V^{max} , are plotted in Fig. 2(g) as a function of τ_M using experimentally determined values for T_1 , V_{rf}^T , V_{rf}^S , and $\sigma(\tau_M)$ [17,18]. The highest visibility, $\geq 90\%$, is realized for $\tau_M \sim 6 \mu\text{s}$.

Previous work using continuous charge sensing showed inhomogeneous dephasing of the $S - T_0$ qubit, which was attributed to precession with a broad frequency spectrum, driven by the fluctuating Overhauser field difference between the two dots [4,19]. For sufficiently fast single-shot repetition, Overhauser fields remain quasistatic over many single-shot measurements, leading to periodic $S - T_0$ precession, as seen in Fig. 3(a). Also evident is a variation of the precession period over ~ 50 ms, reflecting the slowly evolving nuclear environment, consistent with previous measurement and theory [20].

Variation in the $S - T_0$ precession period is more clearly demonstrated in Figs. 3(b) and 3(c). Figure 3(b) shows three sets of precession data taken 10 min apart. Periods of the oscillating triplet probability, P_T , defined by the average of 400 binary outcomes (either S or T_0), correspond to longitudinal Overhauser field differences $\Delta B_z^{\text{nuc}} = 1.3, 1.1, 0.4$ mT (top to bottom). The continuous evolution of the nuclear environment can be seen in Fig. 3(c), which shows P_T as a function of separation time τ_S —each row comparable to a panel in Fig. 3(b), but for τ_S up to 100 ns rather than 500 ns—in slices taken every 100 ms [21]. The meandering light-dark pattern reflects the random evolution of the $S - T_0$ precession period on a

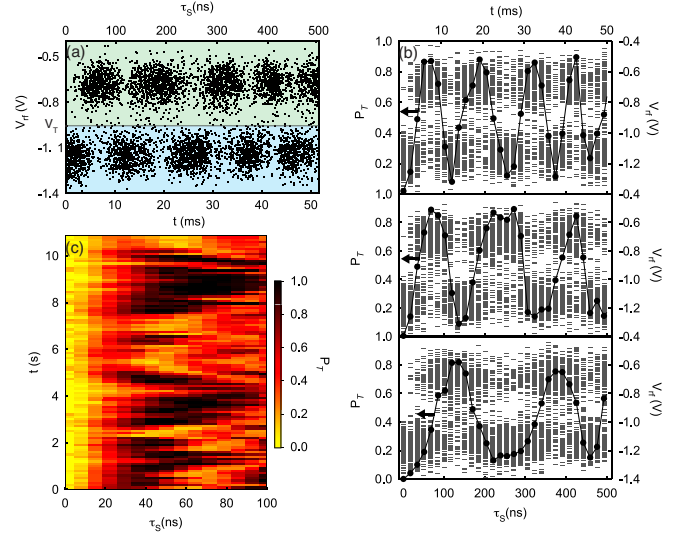


FIG. 3 (color online). (a) 6000 consecutive single-shot $S - T_0$ measurements, V_{rf} , with separation times τ_S stepped by ~ 17 ns every 200 cycles, as a function of overall measurement time, t (bottom axis). Threshold V_T separates outcomes identified as singlet ($V_{\text{rf}} < V_T$) or triplet ($V_{\text{rf}} > V_T$). Oscillations due to Overhauser fields are evident, with slightly evolving period. (b) Single-shot outcomes (gray markers) and triplet probabilities, P_T , (black circles) over τ_S , for three nominally identical runs taken 10 min apart. (c) Rapid acquisition of 108 P_T traces at times t . Probabilities P_T are determined from 400 measurements per τ_S .

~ 1 s time scale, consistent with dipole-dipole mediated nuclear diffusion [20].

Assembling $P_T(\tau_S)$ statistics from single-shot measurements as a function of separation time τ_S yields a time-averaged curve from which an inhomogeneous dephasing time T_2^* can be extracted [4,19]. Each point in Fig. 4(a) is an average over 1600 triplet-state return probabilities, each

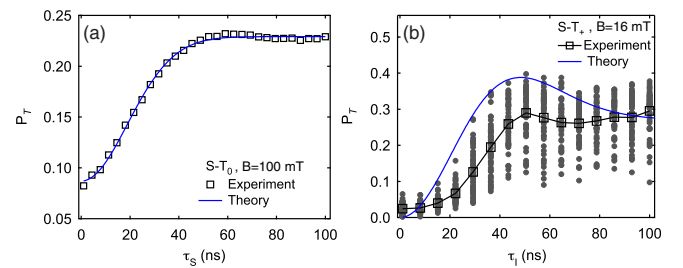


FIG. 4 (color online). (a) Triplet probability P_T as a function of separation time τ_S based on 1600 single-shot measurements per separation time. Fit (blue or gray curve) gives $T_2^* = 27$ ns, $P_T(0) = 1 - F_S = 0.08$, $V = 0.28$ (see text). (b) P_T as a function of separation time τ_I to the $S - T_+$ anticrossing at point I . Probabilities (gray circles) based on 400 single-shot binary measurements. At each τ_I , 50 values of P_T are taken 15 s apart and averaged (open black squares). Theory curve, Eq. 6, yields $B^{\text{nuc}} = 0.7$ mT ($T_2^* = 37$ ns), with relatively poor agreement between experiment and theory (see text).

derived from 400 binary single-shot measurements. The individual $P_T(\tau_S)$ measurements are separated in time by ~ 20 s. A fit to the theoretical Gaussian form, $P_T(\tau_S) = P_T(0) + (V/2)[1 - e^{-(\tau_S/T_2^*)^2}]$, yields $T_2^* = 27$ ns, consistent with previous results [4,20], visibility $V = 0.28$, and intercept $P_T(0) = 1 - F_S = 0.08$. These values yield a reasonable singlet fidelity, $F_S = 0.92$, but relatively low triplet fidelity $F_T = 0.36$ for this data (compared to Figs. 2 and 3) due to a short T_1 in this run.

Finally, we investigate the triplet probability P_T after separating (0,2) singlets to the point I , where the (1,1) singlet state S crosses the T_+ triplet [see Fig. 1(b)]. Whereas mixing of S and T_0 at point S relies on the component of the Overhauser field difference *along* the total field direction, mixing of S and T_+ at point I relies on the component of the Overhauser field difference *transverse* to the total field. Evolution of transverse Overhauser fields are not inhibited by nuclear or electron Zeeman energy differences, and is relatively fast, set by nuclear dipole-dipole (~ 100 μ s) and Knight-shift (~ 10 μ s) energetics [19,20,22,23]. As expected, we do not observe periodic precession between S and T_+ . We note a variation over the course of the measurement in spin-flip probability at a fixed τ_I and separation point I . This is likely due to changes in the position of the narrow $S - T_+$ resonance resulting from a small buildup of nuclear polarization during the measurement [23,24].

Figure 4(b) shows probabilities P_T for the T_+ state as a function of τ_I . Each probability value (gray circle) in Fig. 4(b) is based on 400 binary single-shot measurements with $\tau_M = 8$ μ s. Series of $P_T(\tau_I)$ measurements were made over a range of τ_I up to ~ 100 ns, with an acquisition time ~ 50 ms per series. A total of 50 series, spaced by ~ 15 s to allow decorrelation of longitudinal Overhauser fields, were then averaged to give the black squares in Fig. 4(b).

At small external fields, when the $S - T_+$ anticrossing is in (1,1), the probability of detecting a triplet following separation for a time τ_I can be written $P_T = P_T^0 + V \int d^3\mathbf{B}\rho(\mathbf{B})[(\Delta B_x^2 + \Delta B_y^2)/2(\hbar\omega/|g^*\mu_B|)^2]\sin^2(\omega\tau_I)$, where $\omega = |g^*\mu_B|/(2\hbar)[B_z^2 + 2(\Delta B_x^2 + \Delta B_y^2)]^{1/2}$ is the precession rate between S and T_+ at the center of the anticrossing, $\Delta B_{x(y)} = [B_{x(y)}^L - B_{x(y)}^R]/2$ are transverse Overhauser field differences between left (L) and right (R) dots, $B_z = [B_z^L + B_z^R]/2$ is the average longitudinal Overhauser field, V is readout visibility, and $g^* = -0.44$ is the effective electron g factor in GaAs. Assuming Overhauser fields $\mathbf{B} = (\Delta B_x, \Delta B_y, B_z)$ are Gaussian distributed on long time scales, $\rho(\mathbf{B}) = (2\pi B^{\text{nuc}})^{-3/2} \times e^{-(\mathbf{B}/B^{\text{nuc}})^2/2}$, yields the form in Fig. 4(b) [25]. Setting $P_T^0 = 1 - F_S = 0$ and B^{nuc} to match the overshoot in the data yields $B^{\text{nuc}} = 0.7$ mT $\sim \hbar|g^*\mu_B T_2^*|^{-1}$, corresponding to $T_2^* \sim 40$ ns, and $V = F_T \sim 0.7$. Unlike Fig. 4(a), theory and experiment do not match well for the $S - T_+$ mixing,

due in part to the the buildup of average nuclear polarization, which shifts the $S - T_+$ resonance and lowers P_T .

We acknowledge support from IARPA/ARO, and the Department of Defense. Devices were made at Harvard's Center for Nanoscale Systems (CNS), a member of the NSF National Nanotechnology Infrastructure Network (NNIN). We thank J. M. Taylor, A. C. Doherty, and E. A. Laird for valuable discussion, and J. Waissman for technical assistance.

- [1] D. Loss and D.P. DiVincenzo, Phys. Rev. A **57**, 120 (1998).
- [2] J. Levy, Phys. Rev. Lett. **89**, 147902 (2002).
- [3] D.P. DiVincenzo and D. Loss, Superlattices Microstruct. **23**, 419 (1998).
- [4] J. R. Petta *et al.*, Science **309**, 2180 (2005).
- [5] K. C. Nowack, F. H. L. Koppens, Y. V. Nazarov, and L. M. K. Vandersypen, Science **318**, 1430 (2007).
- [6] M. Pioro-Ladriere *et al.*, Nature Phys. **4**, 776 (2008).
- [7] D. J. Reilly *et al.*, Science **321**, 817 (2008).
- [8] M. A. Armen *et al.*, Phys. Rev. Lett. **89**, 133602 (2002).
- [9] A. Romito, Y. Gefen, and Y. M. Blanter, Phys. Rev. Lett. **100**, 056801 (2008).
- [10] O. Astafiev *et al.*, Phys. Rev. B **69**, 180507 (2004).
- [11] W. Lu *et al.*, Nature (London) **423**, 422 (2003).
- [12] J. M. Elzerman *et al.*, Nature (London) **430**, 431 (2004).
- [13] S. Amasha *et al.*, Phys. Rev. Lett. **100**, 046803 (2008).
- [14] T. Meunier *et al.*, Phys. Rev. B **74**, 195303 (2006).
- [15] D. J. Reilly, C. M. Marcus, M. P. Hanson, and A. C. Gossard, Appl. Phys. Lett. **91**, 162101 (2007).
- [16] A. C. Johnson *et al.*, Nature (London) **435**, 925 (2005).
- [17] For $\tau_M = 1.5$ μ s, $\sigma = 152$ mV. For $\tau_M = 7$ μ s, $\sigma = 82$ mV. For $\tau_M = 15$ μ s, $\sigma = 56$ mV. σ is determined from the control experiment [26]. Other fit parameters: $\Delta V_{\text{rf}} = 0.49$ V, $V_{\text{rf}}^S = -0.40$ V.
- [18] Values for V_{rf}^S and ΔV_{rf} are fit once using the 15 μ s data in Fig. 2(e). The value $T_1 = 34$ μ s and $\langle P_T \rangle = 0.5$ are from a fit to the relaxation data in Fig. 2(c). Note that $\langle P_T \rangle \sim 0.5$ is the theoretically expected value.
- [19] J. M. Taylor *et al.*, Phys. Rev. B **76**, 035315 (2007).
- [20] D. J. Reilly *et al.*, Phys. Rev. Lett. **101**, 236803 (2008).
- [21] Each P_T value (pixel) in Fig. 3(c) is based on 1000 single-shot measurements. Each row of 15 probabilities is acquired in 80 ms, followed by 20 ms of dead time. For these measurements, $B = 100$ mT.
- [22] R. Hanson *et al.*, Rev. Mod. Phys. **79**, 1217 (2007).
- [23] J. M. Taylor, Ph.D. thesis, Harvard University, 2007.
- [24] J. R. Petta *et al.*, Phys. Rev. Lett. **100**, 067601 (2008).
- [25] This form is expected to apply at low applied magnetic field, where the $S - T_+$ anticrossing is in (1,1). See Eqs. (7.1)–(7.3) in Ref. [23]. See EPAPS Document No. E-PRLTAO-103-020943 for a derivation of this equation. For more information on EPAPS, see <http://www.aip.org/pubservs/epaps.html>.
- [26] A background slope of V_{rf} with τ_S , due to a $\sim \mu$ V gate voltage shift of point M with changing τ_S , is subtracted. The slope is determined from a control experiment with M outside the (1,1) metastability region.